

Article

Effects of Al₂O₃ Thickness in Silicon Heterojunction Solar Cells

Doowon Lee ^{1,†}, Myoungsu Chae ^{1,†} , Jong-Ryeol Kim ² and Hee-Dong Kim ^{1,*}

¹ Department of Semiconductor Systems Engineering and Convergence Engineering for Intelligent Drone, Institute of Semiconductor and System IC, Sejong University, 209, Neungdong-ro, Gwangjin-gu, Seoul 05006, Republic of Korea

² Department of Optical Engineering, Sejong University, 209, Neungdong-ro, Gwangjin-gu, Seoul 05006, Republic of Korea

* Correspondence: khd0708@sejong.ac.kr

† These authors contributed equally to this work.

Abstract: In this paper, we investigate the effects of aluminum oxide (Al₂O₃) antireflection coating (ARC) on silicon heterojunction (SHJ) solar cells. Comprehensive ARCs simulation with Al₂O₃/ITO/c-Si structure is carried out and the feasibility to improve the short circuit current density (J_{SC}) is demonstrated. Based on the simulation results, we apply Al₂O₃ ARC on SHJ solar cells, and the increment in J_{SC} to 1.5 mA/cm² is observed with an Al₂O₃ layer thickness of 20 nm. It is because the total reflectance of SHJ solar cells is decreased by the shifting of the wavelength range on constructive and destructive light interference. As a result, we believe that the proposed Al₂O₃ ARC can support an effective engineering technic to increase J_{SC} and efficiency of SHJ solar cells.

Keywords: Al₂O₃; antireflection coating; SHJ solar cell; external quantum efficiency

1. Introduction

Reducing the levelized cost of energy (LCOE) is a value used to compare the cost of producing energy from various sources over the lifespan of a power station. In recent years, renewable energy sources such as wind, solar, hydro, and geothermal have grown more competitive owing to technological advancements and economies of scale. The LCOE of renewable energy varies based on location, resource availability, financing costs, and used technology, among other different factors. In general, however, the LCOE of renewable energy has been decreasing, making it more cost-competitive with power derived from fossil fuels. LCOE of crystalline silicon (c-Si) solar cells is essential in order to replace existing energy technologies such as nuclear and coal power plants [1]. Several types of c-Si solar cells have been or are being developed to decrease the LCOE by decreasing the manufacturing cost and increasing light conversion efficiency [2]. These include passivated emitter solar cells (PESCs) [3], passivated emitter and rear cells (PERCs) [4], interdigitated back-contact (IBC) solar cells [5], passivated emitter rear-locally diffused cells (PERLs) [6,7], and heterojunction c-Si (SHJ) solar cells [3]. Among them, SHJ solar cells have demonstrated efficiencies of up to 26.7% [4], making them strong candidates for reducing LCOE. Even though the SHJ solar cell shows high efficiency, the technologies to increase its efficiency should be studied to decrease LCOE.

In order to increase the efficiency of SHJ solar cells, many technologies to improve solar cell parameters, such as short circuit current density (J_{SC}), open circuit voltage (V_{OC}), and fill factor (FF) have been proposed. Surface passivation of SHJ solar cells is crucial to reduce carrier recombination and improve their V_{OC}. Amorphous Si is used as a passivation layer in SHJ solar cells to improve them. It is also used as a carrier-selective layer, which helps to separate the electrons and holes in the SHJ solar cell efficiency [8]. In order to get a high V_{OC} in SHJ solar cells, optimizing amorphous Si is essential. J. Sritharathikhun et al. investigated the use of intrinsic hydrogenated amorphous Si oxide as a buffer layer in the interplay with



Citation: Lee, D.; Chae, M.; Kim, J.-R.; Kim, H.-D. Effects of Al₂O₃ Thickness in Silicon Heterojunction Solar Cells. *Inorganics* **2023**, *11*, 106. <https://doi.org/10.3390/inorganics11030106>

Academic Editor: Catherine Housecroft

Received: 19 January 2023

Revised: 27 February 2023

Accepted: 2 March 2023

Published: 4 March 2023



Copyright: © 2023 by the authors. Licensee MDPI, Basel, Switzerland. This article is an open access article distributed under the terms and conditions of the Creative Commons Attribution (CC BY) license (<https://creativecommons.org/licenses/by/4.0/>).

doped microcrystalline Si oxide layers to improve the efficiency of SHJ solar cells [9]. Post-deposition argon plasma treatment was also demonstrated to improve the amorphous Si passivation layer for SHJ solar cells [8]. Meanwhile, in order to increase FF, researchers are investigating ways to decrease series resistance in SHJ solar cells. One study used several approaches to obtain a low series resistance for a state-of-the-art 2 cm × 2 cm screen-printed solar cell reaching 82.5% FF. [10]. Research related to copper plating is also conducted in the metallization of SHJ solar cells because the performance of the copper-plated solar cell showed enhanced characteristics as compared to that of a reference solar cell built by silver screen printing. Especially, because copper plating has enormous advantages such as low cost, improving J_{SC} by fine line plating, and a low temperature process, copper-plating on SHJ solar cells has attracted the attention of many researchers. A new plated metallization process for SHJ solar cells involves selective plating of copper onto a positively masking seed [11]. Researchers have developed a laser-based method for the metallization of SHJ solar cells by copper-plating [12]. Selective copper electroplating without any resist-mask is also being developed for SHJ solar cells [13]. In addition, studies related to the seed layer were also investigated and reported decreased series resistance [14]. In terms of studies related to J_{SC} , one of the most promising research trends in improving J_{SC} for SHJ solar cells is anti-reflection coating (ARC) by using the development of new materials and structures that can enhance light trapping and absorption in SHJ solar cells [15–17]. For instance, researchers have investigated the use of nanoparticle coatings, plasmonic structures, and microtextured surfaces to improve the light absorption of SHJ solar cells. In laboratory tests, these methods have demonstrated promise, but additional study is required to optimize their efficacy and scale up their production. Integration of many layers of coatings to improve light absorption and minimize reflection is another significant development in SHJ solar cell research. Researchers have created multilayer antireflective coatings (DLARCs) that use a combination of dielectric and metallic layers to reduce reflection over a broad spectrum of wavelengths [18,19]. These multilayer coatings can increase the efficiency of SHJ solar cells by up to 20%, making them extremely promising for commercial use [20]. In addition to the optimization of materials and structures, there has been extensive research into the creation of cost-effective and scalable production procedures for ARCs. For instance, researchers have investigated the use of sol-gel processes, electrochemical deposition, and printing methods to create extremely efficient and inexpensive ARCs [21,22]. These strategies could drastically cut the cost of solar cell production and increase solar energy's accessibility to a wider spectrum of consumers. Among various technologies, ARC on indium tin oxide (ITO) have attracted attention due to its possibility to increase J_{SC} and reliability of the solar cell. Improved J_{SC} was demonstrated by employing indium zinc oxide (IZO)/ITO stacked structure [23]. A HfO₂-deposited SHJ solar cell also exhibited high current density [24]. Yamamoto et al. reported that the J_{SC} and reliability of a SHJ solar cell was increased via deposition of a silicon dioxide (SiO₂) layer [25]. Although the possibility of SiO₂ ARC on SHJ solar cell has been demonstrated by several institutes, it requires relative thickness of 84 nm [24], which could lead to the degradation of passivation quality and efficiency during the deposition. Therefore, ARC studies, which feature a thin insulator, should be conducted.

Aluminum oxide (Al₂O₃), which is widely used in the c-Si solar cell industry, can be one of the candidates for ARC [26–28]. In the reported literature, the possibility of Al₂O₃ ARC to increase J_{SC} has been shown with thinner thickness of 35 nm [24], while it was not demonstrated yet. Therefore, in the present study, we investigate the influence of Al₂O₃ ARC on SHJ solar cell. Figure 1 shows schematic structure of the SHJ solar cell with Al₂O₃ and brief mechanism of it, indicating that the interference of the reflected lights can decrease the total reflectance, resulting in the increase of J_{SC} . In order to evaluate its feasibility, ARC characteristics of Al₂O₃ were analyzed where the configuration of the Al₂O₃ and ITO layer thickness and the ITO dopant concentration that afforded the highest J_{SC} was identified. Based on the results of the simulations, we experimentally demonstrated SHJ solar cells

with an Al_2O_3 layer of various thicknesses in SHJ solar cells and analyzed the properties of the cells.

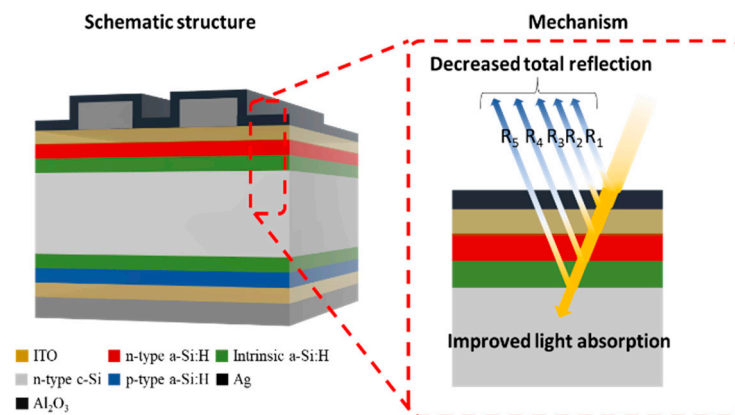


Figure 1. Schematic structure of the proposed SHJ solar cell with an Al_2O_3 layer.

2. Materials and Methods

In order to analyze the effects of Al_2O_3 , OPAL 2 program is employed because it is a simulation program designed for the study of ARC [29]. The program employs a complex algorithm to evaluate the dependence of refractive index on wavelength [30]. The light-trapping model is expressed by $Z = 4 + \{\ln[n^2 + (1 - n^2) \times \exp^{-4\alpha W}]\} / \alpha W$ where Z is the optical pathlength, n is the refractive index of the ARC, α is the polarization angle, and W is the thickness of the substrate.

The air/ Al_2O_3 / ITO/Si substrate structure is used in our OPAL 2 simulations. A 180- μm thick c-Si substrate was selected, and random upright pyramids with a characteristic angle of 54.74° were applied as texture structures. The dopant concentration in the ITO layer on the c-Si substrate was set to 2.0×10^{20} , 4.9×10^{20} , and $6.0 \times 10^{20} / \text{cm}^3$. The ‘ Al_2O_3 on glass (Kum09)’ option was selected for the Al_2O_3 layer. AM 1.5 G was selected for incident illumination at a 0° zenith angle to the normal of the plane of the cell. The total current density from the light source was fixed at $44 \text{ mA}/\text{cm}^2$. The reflected current density (J_R), the absorbed current density in the Al_2O_3 and ITO layers (J_A), and the absorbed current density in the c-Si (generation current density, J_G) were analyzed. The dependence of current density on the Al_2O_3 and ITO layer thickness and the ITO dopant concentration was evaluated, and the relationship between reflectance and wavelength was determined.

Amorphous i/n-type and i/p-type Si layers were applied to the substrates via plasma-enhanced chemical vapor deposition (PECVD, PlasmaPro System100, Oxford Instruments, Abingdon, UK). ITO layers 80 nm thick were deposited by using sputter (KVS-2000L, Korea Vacuum Tech, Gimpo-si, Republic of Korea) on the n- and p-type layers. Ag evaporation via e-beam evaporator with deposition rate of $0.5 \text{ \AA}/\text{s}$ was performed following a photolithography process. Al_2O_3 was deposited by atomic layer deposition (ALD, THECO 200M, WONIK IPS, Pyongtaek, Republic of Korea) using trimethylaluminium (TMA) and O_2 plasma as precursor and oxidant, respectively. The ALD was heated up to 250°C , and the thickness of Al_2O_3 was controlled by the number of deposition cycles. In order to investigate the possibility to improve J_{SC} , the reflectance of the SHJ solar cell with Al_2O_3 layer was measured by UV-visible spectroscopy (Cary-5000, Agilent Technologies, Santa Clara, CA, USA) and weighted reflectance was calculated from the measured reflectance data by the equation as follows. Solar-weighted $R = (\int(S(\lambda) \times R(\lambda) \times \Delta\lambda)) / (\int(S(\lambda) \times \Delta\lambda))$, where $R(\lambda)$ is the measured reflectance, and S_λ is the solar irradiance (AM 1.5 G) [31]. In order to investigate the effect of Al_2O_3 ARC directly on SHJ solar cell, the solar cell parameters were measured before and after Al_2O_3 deposition under illumination with a solar simulator (K201-LAB 50, McScience, Suwon, Republic of Korea). In addition, the external quantum

efficiency (EQE) of each cell before and after Al₂O₃ deposition was measured to compare ARC performance.

3. Results

In order to investigate the influence of Al₂O₃ on SHJ solar cell, the dependence of J_G the Al₂O₃ and ITO layer thickness and the ITO dopant concentration is investigated, as shown in Figure 2. Trend of J_G was generally increased when the Al₂O₃ and ITO layer was thick and thin, and the maximum J_G was 43.12 mA/cm² for all dopant concentration. In the case of ITO dopant concentration of 2.1×10^{20} /cm³, the maximum J_G was observed as the thickness of Al₂O₃ and ITO was 70 and 30 nm. In the case of ITO dopant concentration of 4.9×10^{20} and 6.1×10^{20} /cm³, the maximum J_G was observed with the structure without ITO. In order to obtain the proper electric conductivity for the SHJ solar cells, the thickness of the ITO layer have to resemble that of an actual solar cell. The ITO layer in an actual SHJ cell is typically 50–100 nm thick [25]. So as to analyze the influence of Al₂O₃ to the practical SHJ solar cell, the optimized ITO thickness was obtained via the Air/ITO/c-Si structure without Al₂O₃. The optimized ITO thickness without Al₂O₃ to maximize J_G was 68, 63, and 59 nm for the ITO dopant concentration of 2.1×10^{20} , 4.9×10^{20} , and 6.1×10^{20} /cm³. Based on the optimized ITO, the influence of Al₂O₃ thickness was then analyzed.

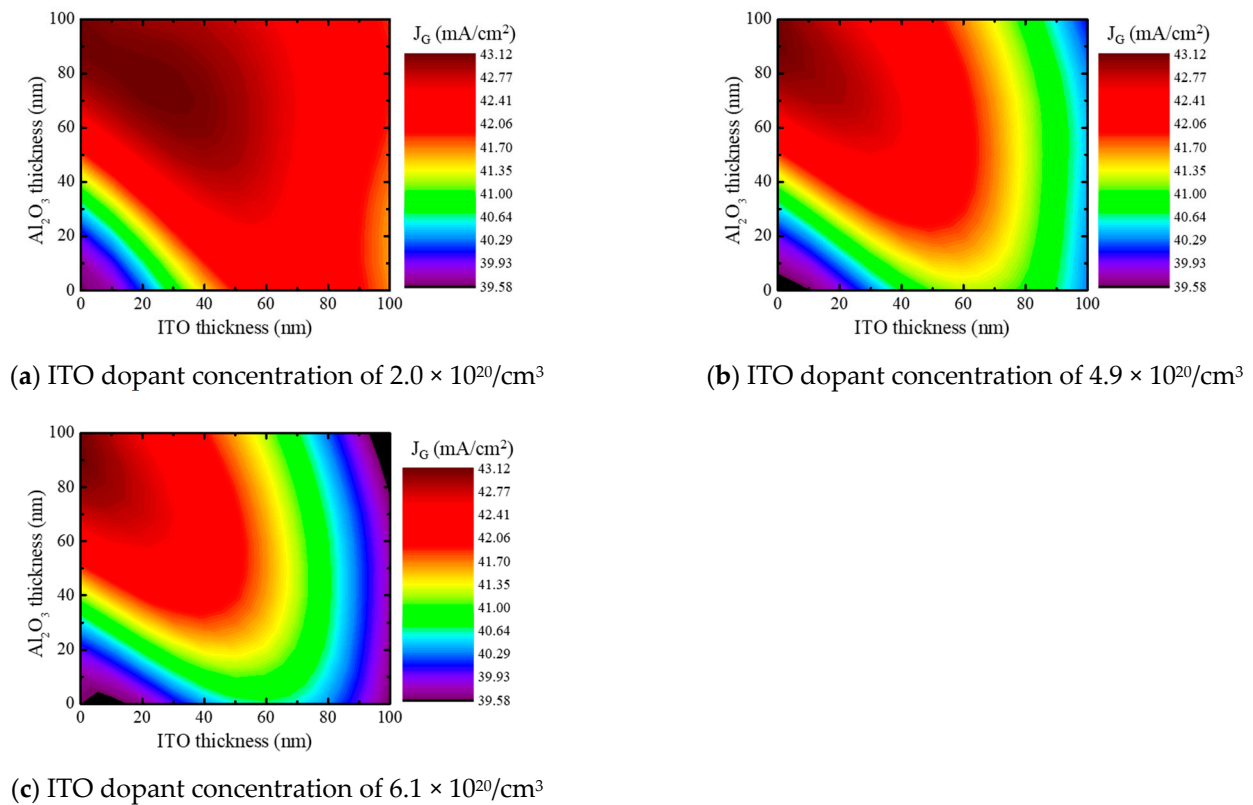


Figure 2. J_G characteristics performed with the Al₂O₃/ITO/c-Si structure via OPAL 2 simulation. The dependence of J_G on ITO dopant concentration and Al₂O₃ thickness is shown. ITO dopant concentration: (a) 2.0×10^{20} , (b) 4.9×10^{20} , and (c) 6.1×10^{20} /cm³.

Figure 3 shows the J_G, J_R, and J_A depending on the thickness of Al₂O₃ and doping concentrations of ITO. At an ITO dopant concentration of 2.0×10^{20} /cm³, J_G increased from 42.26 to 42.60 mA/cm² when a 68 nm-thick Al₂O₃ layer was deposited on the optimized ITO. At an ITO dopant concentration of 4.9 and 6.1×10^{20} /cm³, the deposition of 52 and 50 nm-thick Al₂O₃ layer for each concentration yielded an increased J_G from 41.19 and 40.64 to 41.93 and 41.67 mA/cm². The J_G, however, was decreased as the thickness of Al₂O₃ was continuously increased. In addition, all simulation results indicated that

the J_A manifested minor changes with respect to the thickness of Al_2O_3 , whereas J_G was dominantly affected by J_R . In order to investigate the change in the reflectance in detail, we investigated the reflectance according to wavelength, as shown in Figure 4. At an ITO dopant concentration of $2.0 \times 10^{20}/cm^3$, reflectance of light at wavelengths from 400 to 700 nm was increased by Al_2O_3 deposition, whereas the reflectance of wavelengths in other range was reduced, as shown in Figure 4a. At ITO dopant concentrations of 4.9×10^{20} and $6.1 \times 10^{20}/cm^3$, the trends of increased and decreased reflectance at each wavelength range were similar to that observed with $2.0 \times 10^{20}/cm^3$ ITO dopant, as shown in Figure 4b,c. It is because the construction and destruction interference at wavelengths was shifted after deposition of Al_2O_3 , which corresponded to the literatures [23,24]. In detail, it was due to the effects of ARCs. ARCs are thin films put on a material's surface to reduce the amount of light reflected at the interface of materials and a substrate. These coatings are intended to match the refractive index of the material with that of a substrate, hence decreasing surface reflection. The antireflection coating's thickness is crucial to its efficiency, and it must be properly regulated to obtain the necessary amount of reflection reduction. Single layer antireflection coatings, which is commonly used, consist of a single thin film deposited on a Si wafer. The thickness of the film is chosen to minimize the reflection at a specific wavelength, which is usually the wavelength of the light source being used for SHJ solar cells. The refractive index of the film is also carefully selected to match the refractive index of a Si wafer. For SHJ solar cells, the thicknesses of the ITO and amorphous i/n-type Si layers are optimized to minimize reflections in the visible light region from the front. In general, researchers want to get the lowest reflectance in the visible range because that is where the intensity of light is the strongest, resulting in enabling to maximize the efficiency of the solar cell. As shown in Figure 4, the lowest reflectance was thus observed in the wavelength range between 400 and 600 nm when only the ITO was deposited. However, as the industry demands higher efficiency from solar cells, DLARCs technology is being used to further minimize the reflections. In a DLARC, two thin films of materials with different refractive indices are typically placed on a substrate. Thickness of each layer is carefully selected so that the two layers interact in a manner that cancels out the reflections that would be generated by each layer independently. As a result of the interaction, the result is an exceptionally low degree of reflection across a broad spectrum of wavelengths. The main concept underlying DLARCs is construction and destruction interference of light. Light interacts with the atoms and molecules that make up a substance as it passes through it. Consequently, the velocity of the light changes, causing it to bend or refract. The degree of bending depends on the refractive index of the materials. The refractive indices of the two layers of material in a double-layer antireflection coating are different. When light passes from one material to another, light interacts with both layers, resulting in the reflectance change with respect to the wavelength. In Figure 4b, we observed the change in reflectance for each wavelength after the deposition of Al_2O_3 as above. This was due to the interaction between the light reflected from the Al_2O_3 and the light reflected from the ITO as the Al_2O_3 was deposited, as mentioned above. The trend of reflectance was also changed as the thickness of the Al_2O_3 increased, indicating that to maximize the efficiency of the solar cell, the thickness of each layer must be adjusted so that the light reflected by one layer adequately interferes with the light reflected by the other layer. Accordingly, the simulation results demonstrated that Al_2O_3 layer of a certain thickness can improve the J_G , and the ITO dopant concentration had an effect on the J_G as well.

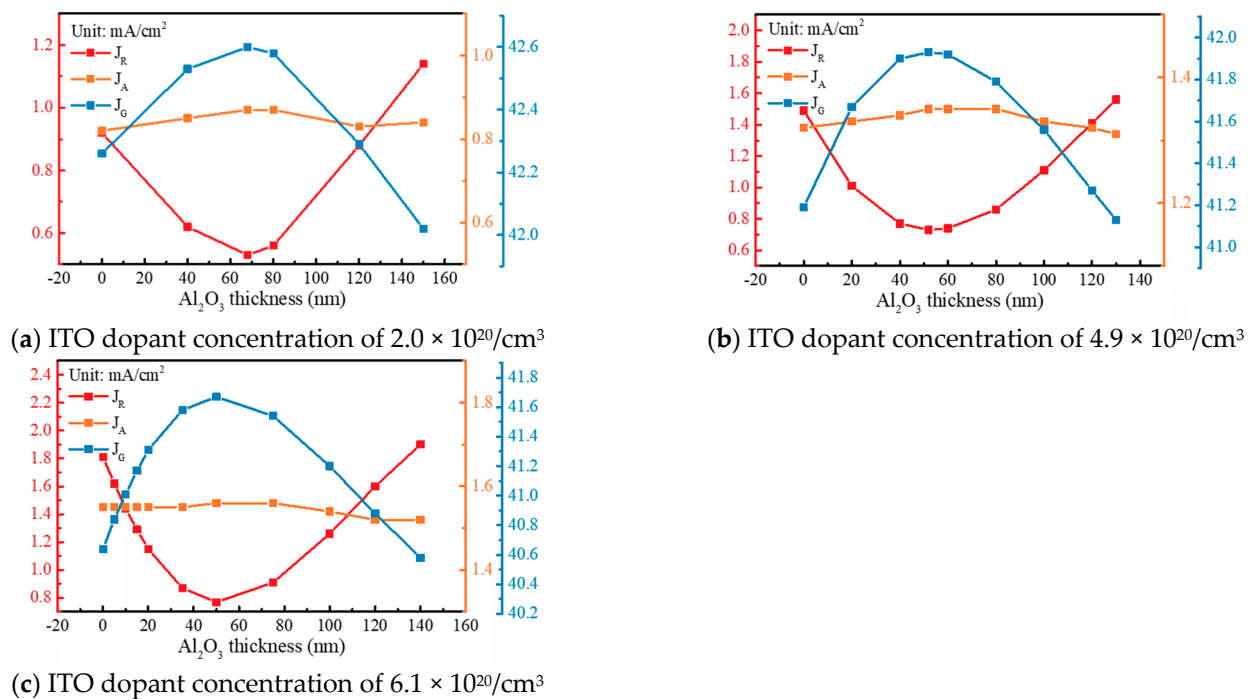


Figure 3. Current density performed with the Al₂O₃/ITO/Si structure via OPAL 2 simulation. J_R, J_A, and J_G are plotted against Al₂O₃ layer thickness at different ITO dopant concentrations. ITO dopant concentration: (a) 2.0×10^{20} , (b) 4.9×10^{20} , and (c) $6.1 \times 10^{20}/\text{cm}^3$.

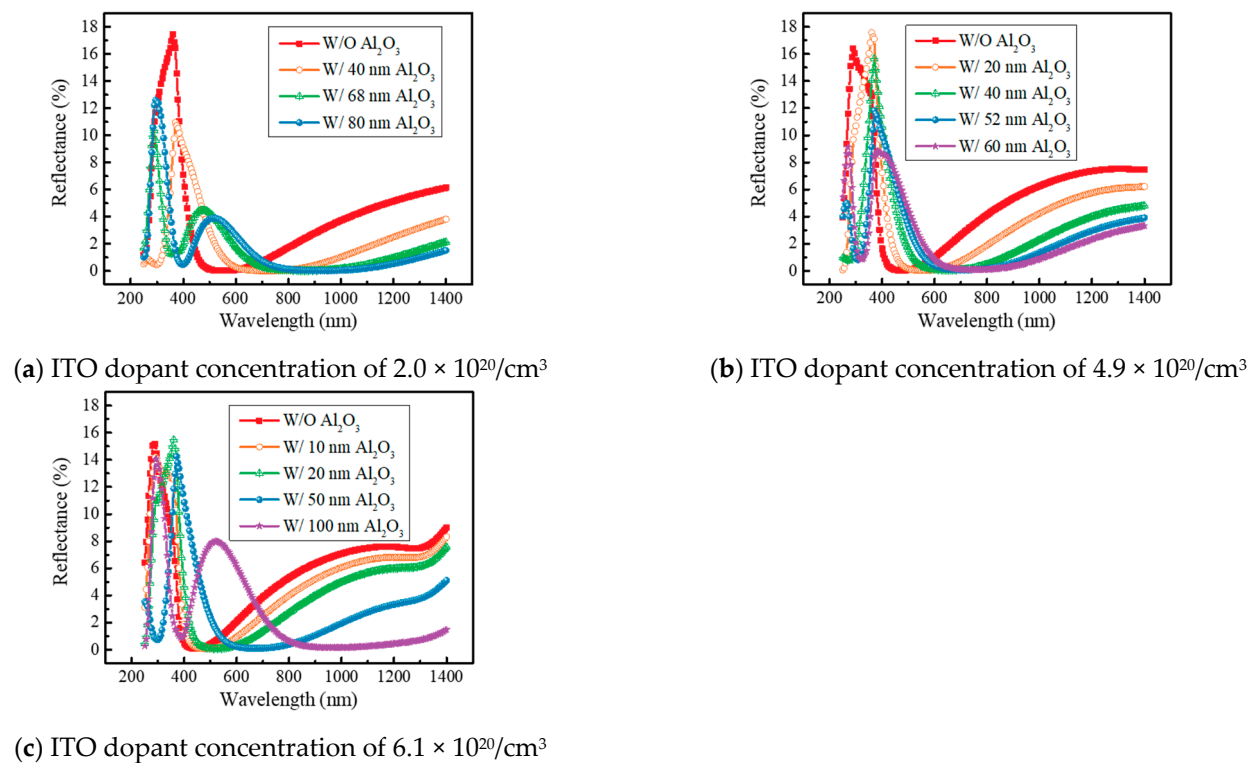


Figure 4. Reflectance results performed with the Al₂O₃/ITO/Si structure via OPAL 2 simulation. The dependence of reflectance on Al₂O₃ layer thickness at different ITO dopant concentrations is shown. ITO dopant concentration: (a) 2.0×10^{20} , (b) 4.9×10^{20} , and (c) $6.1 \times 10^{20}/\text{cm}^3$.

In order to investigate the influence of Al₂O₃ ARC, reflectance was first measured, and the weighted reflectance was calculated from the measured reflectance because it was used to estimate the feasibility of the ARCs with respect to the intensity of solar irradiation [5]. Measured reflectance and weighted reflectance according to Al₂O₃ thickness are shown in Figure 5. The results of the reflectance measurements were similar to the simulation results. Reflectance in the wavelength range from ~400 nm to 600 nm increased, but it decreased at shorter and longer wavelengths ranges, as shown in Figure 5. As thickness of Al₂O₃ was increased, the increase and decrease in reflectance were enhanced. The inset figure in Figure 5 shows the calculated weighted reflectance depending on the thickness of Al₂O₃, indicating that the weighted reflectance was decreased from 4.03% to 3.72% at Al₂O₃ thickness of 25 nm. However, the weighted reflectance increased to 4.05% when the thickness of the deposited Al₂O₃ layer was increased to 30 nm. These reflectance changes were seen because the total reflectance with respect to the wavelength changed by the deposition Al₂O₃, which corresponded with the simulation result.

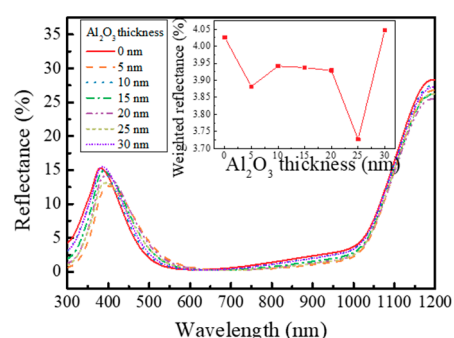


Figure 5. Reflectance from fabricated Al₂O₃-deposited SHJ solar cells where the inset figure shows calculated weighted reflectance.

To investigate the effect of Al₂O₃ on SHJ solar cell parameter directly, we measured EQE, J_{SC}, V_{OC}, and FF before and after Al₂O₃ deposition. The EQEs with Al₂O₃ layer thicknesses of 5, 10, 15, 20, 25, and 30 nm from 300 to 1100 nm are shown in Figure 6. Commonly, we observed that reflectance decreased at wavelengths from ~420 nm to 600 nm and increased at longer and shorter wavelengths. By comparing Figures 5 and 6, the wavelength range, which manifested the improved EQE, was similar with the wavelength range where reflectance was decreased for all solar cells. Accordingly, we observed the change of the reflectance by deposition of Al₂O₃ which was similar with the simulation results, indicating that it can improve the efficiency. In order to investigate the influence of Al₂O₃ ARC directly, the SHJ solar cell parameters before and after deposition of Al₂O₃ are summarized in Table 1. J_{SC} of the cell with a 5 nm-thick Al₂O₃ layer was 1.0 mA/cm² higher than J_{SC} of the cell prior to Al₂O₃ deposition. Compared to the J_{SC} of cells prior to Al₂O₃ deposition, J_{SC} of the cells with Al₂O₃ layers 10, 15, 20, 25, and 30 nm thick was higher by 1.25, 1.0, 1.5, 1.25, and 1.25 mA/cm², respectively. Thus, the J_{SC} of all cells was increased by deposition of Al₂O₃. The highest increase of 1.5 mA/cm² in J_{SC} was observed when 20 nm-thick Al₂O₃ was deposited on SHJ solar cell. Compared to HfO₂ and IZO layer on ITO, it showed an increased J_{SC} of 0.84 and 1 mA/cm². As a result, we obtain the highest improvement in the efficiency from 22% to 23% by deposition of a 20 nm-thick Al₂O₃ on SHJ solar cell. Figure 7 shows the current–voltage (I–V) curve of the SHJ solar cell before and after the Al₂O₃ deposition, indicating that the J_{SC} increased after the Al₂O₃ deposition.

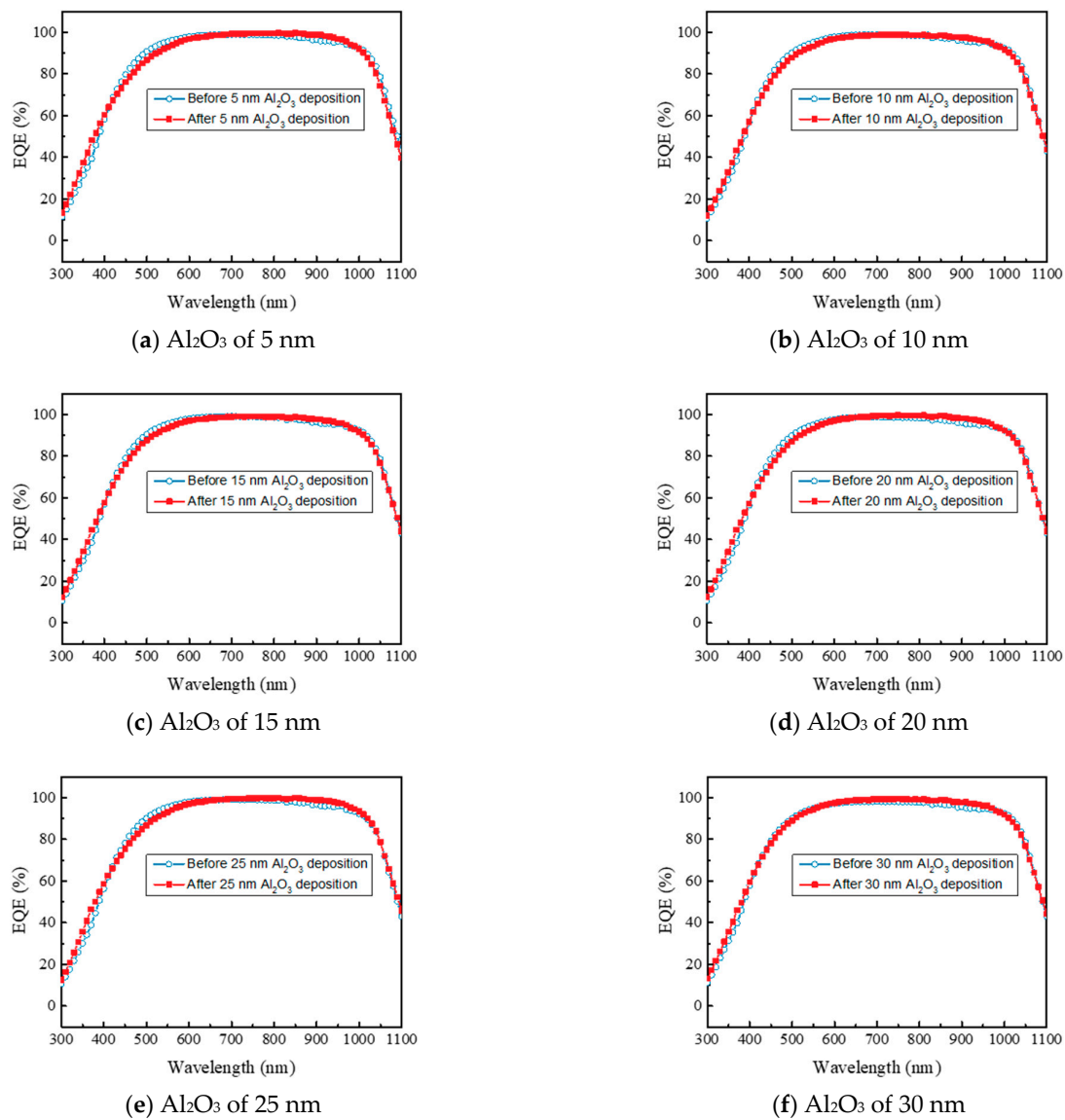


Figure 6. EQE of SHJ solar cell with Al₂O₃ of (a) 5, (b) 10, (c) 15, (d) 20, (e) 25, and (f) 30 nm. EQE measured before Al₂O₃ deposition is also shown.

Table 1. Results of solar simulator before and after Al₂O₃ deposition.

Thickness (nm)	Before/After Deposition	V _{oc} (mV)	J _{sc} (mA/cm ²)	FF (%)	Efficiency (%)
5	Before	712	40.5	75.4	21.74
	After	704	41.5	71	20.74
10	Before	709	40.5	74.9	21.51
	After	706	41.75	72.9	21.59
15	Before	711	40.5	76.1	21.91
	After	708	41.5	72.3	21.24
20	Before	714	40.5	76.1	22.01
	After	715	42	76.6	23.00
25	Before	711	40.25	75.1	21.49
	After	710	41.5	76.4	22.51
30	Before	713	40.5	76.2	22.00
	After	712	41.75	75.7	22.50

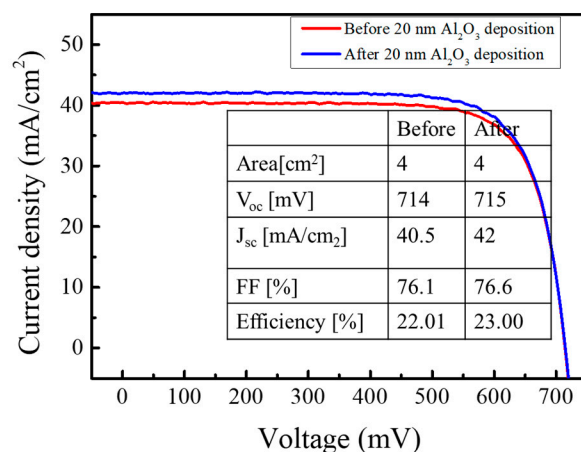


Figure 7. J–V curves of the SHJ solar cell before and after deposition of 15 nm Al₂O₃, with an Al₂O₃ layer.

4. Conclusions

In this paper, we analyze the influence of Al₂O₃ ARC on SHJ solar cells with OPAL2 simulation and by employing it in SHJ solar cells. Feasibility of the Al₂O₃ ARC was demonstrated via OPAL 2 simulation, which indicated that the J_{SC} can be affected by the thickness of Al₂O₃ and the ITO dopant concentration. The J_G was found to be 43.12 mA/cm² for all dopant concentration. The study revealed that to obtain the proper electric conductivity for SHJ solar cells, the thickness of the ITO layer should resemble that of an actual solar cell, which is typically 50–100 nm thick. The optimized ITO thickness without Al₂O₃ was found to be 68, 63, and 59 nm for different ITO dopant concentrations. After determining the optimized ITO thickness, the impact of Al₂O₃ thickness was analyzed. The results showed that at ITO dopant concentration of $2.0 \times 10^{20}/\text{cm}^3$, J_G increased from 42.26 to 42.60 mA/cm² when a 68 nm-thick Al₂O₃ layer was deposited on the optimized ITO. However, the J_G decreased as the thickness of Al₂O₃ was continuously increased. Additionally, the study found that the J_A manifested minor changes with respect to the thickness of Al₂O₃, whereas J_G was dominantly affected by J_R. Finally, the authors analyzed the reflectance of light according to wavelength and found that the lowest reflectance was observed in the wavelength range between 400 and 600 nm when only the ITO was deposited. DLARCs technology was demonstrated for further minimizing reflections to increase the efficiency of the solar cell. Based on the simulation, we compared the solar cell parameters before and after Al₂O₃ deposition. For all SHJ solar cells, when Al₂O₃ was deposited, the reflectance in the wavelengths from 400 to 600 nm was increased, while that in the other wavelengths range was decreased. These reflectance changes showed an effect in the total reflectance changes, resulting in changes in the J_{SC}. The maximum increase in J_{SC} of 1.5 mA/cm² was observed in the cell with a 20 nm-thick Al₂O₃ layer, resulting in the highest efficiency of 23%. The J–V curve of the SHJ solar cell before and after the Al₂O₃ deposition showed an increase in J_{SC} after the deposition. Accordingly, Al₂O₃ deposition can be a steppingstone to improve the current density as well as the reliability of the solar cell modules.

Author Contributions: Conceptualization, D.L.; methodology D.L.; validation, M.C.; formal analysis, D.L. and M.C.; investigation, D.L. and M.C.; resources, H.-D.K.; data curation, D.L. and M.C.; writing—original draft preparation, D.L.; writing—review and editing, J.-R.K. and H.-D.K.; visualization, D.L., M.C., J.-R.K. and H.-D.K.; supervision, H.-D.K.; project administration, H.-D.K.; funding acquisition, H.-D.K. All authors have read and agreed to the published version of the manuscript.

Funding: The research was supported his work was supported in part by the Basic Science Research Program via the National Research Foundation of Korea (NRF) funded by the Ministry of Education under Grant NRF-2020R1F1A1048423 and Grant 2022R1F1A1060655, and in part by the Korea Institute for Advancement of Technology (KIAT) funded by the Korean Government (MOTIE) through the Competency Development Program for Industry Specialist under Grant P0020966.

Data Availability Statement: Data sharing is not applicable to this article as no new data were created or analyzed in this study.

Conflicts of Interest: The authors declare no conflict of interest.

References

1. Fthenakis, V.; Mason, J.E.; Zweibel, K. The technical, geographical, and economic feasibility for solar energy to supply the energy needs of the US. *Energy Policy* **2009**, *37*, 387–399. [\[CrossRef\]](#)
2. Branker, K.; Pathak, M.J.M.; Pearce, J.M. A review of solar photovoltaic levelized cost of electricity. *Renew. Sustain. Energy Rev.* **2011**, *15*, 4470–4482. [\[CrossRef\]](#)
3. Green, M.A.; Blakers, A.W.; Shi, J.; Keller, E.M.; Wenham, S.R. 19.1% efficient silicon solar cell. *Appl. Phys. Lett.* **1984**, *44*, 1163–1164. [\[CrossRef\]](#)
4. Yoshikawa, K.; Kawasaki, H.; Yoshida, W.; Irie, T.; Konishi, K.; Nakano, K.; Uto, T.; Adachi, D.; Kanematsu, M.; Uzu, H.; et al. Silicon heterojunction solar cell with interdigitated back contacts for a photoconversion efficiency over 26%. *Nat. Energy* **2017**, *2*, 17032. [\[CrossRef\]](#)
5. Benick, J.; Richter, A.; Müller, R.; Hauser, H.; Feldmann, F.; Krenckel, P.; Riepe, S.; Schindler, F.; Schubert, M.C.; Hermle, M.; et al. High-efficiency n-type HP mc silicon solar cells. *IEEE J. Photovolt.* **2017**, *7*, 1171–1175. [\[CrossRef\]](#)
6. Green, M.A. The path to 25% silicon solar cell efficiency: History of silicon cell evolution. *Prog. Photovoltaics Res. Appl.* **2009**, *17*, 183–189. [\[CrossRef\]](#)
7. Zhao, J.; Wang, A.; Green, M. 24% efficient PERL structure silicon solar cells. In Proceedings of the Photovoltaic Specialists Conference, Kissimmee, FL, USA, 21–25 May 1990; Conference Record of the Twenty First IEEE; IEEE: Piscataway, NJ, USA, 1990; pp. 333–335.
8. Neumüller, A.; Sergeev, O.; Heise, S.J.; Bereznev, S.; Volobujeva, O.; Salas, J.F.L.; Vehse, M.; Agert, C. Improved amorphous silicon passivation layer for heterojunction solar cells with post-deposition plasma treatment. *Nano Energy* **2018**, *43*, 228–235. [\[CrossRef\]](#)
9. Sritharathikhun, J.; Yamamoto, H.; Miyajima, S.; Yamada, A.; Konagai, M. Optimization of Amorphous Silicon Oxide Buffer Layer for High-Efficiency p-Type Hydrogenated Microcrystalline Silicon Oxide/n-Type Crystalline Silicon Heterojunction Solar Cells. *Jpn. J. Appl. Phys.* **2008**, *47*, 8452–8455. [\[CrossRef\]](#)
10. Antognini, L.; Senaud, L.-L.; Türkay, D.; Marthey, L.; Dréon, J.; Paviet-Salomon, B.; Despeisse, M.; Boccard, M.; Ballif, C. Contact resistivity measurements and their applicability for accurate series resistance breakdown in heterojunction solar cell. *AIP Conf. Proc.* **2022**, *2487*, 020002.
11. Rohit, R.; Rodofili, A.; Cimiotti, G.; Bartsch, J.; Glatthaar, M. Selective plating concept for silicon heterojunction solar cell metallization. *Energy Procedia* **2017**, *124*, 901–906. [\[CrossRef\]](#)
12. Aguilar, A.; Herasimenka, S.Y.; Karas, J.; Jain, H.; Lee, J.; Munoz, K.; Michaelson, L.; Tyson, T.; Dauksher, W.J.; Bowden, S. Development of Cu plating for silicon heterojunction solar cells. In Proceedings of the 2016 IEEE 43rd Photovoltaic Specialists Conference (PVSC), Portland, OR, USA, 5–10 June 2016; IEEE: Piscataway, NJ, USA, 2016; pp. 1972–1975.
13. Hatt, T.; Bartsch, J.; Franzl, Y.; Kluska, S.; Glatthaar, M. Advances with resist-free copper plating approaches for the metallization of silicon heterojunction solar cells. *AIP Conf. Proc.* **2019**, *2156*, 020010.
14. Lee, S.H.; Lee, D.W.; Lee, S.H.; Park, C.K.; Lim, K.J.; Shin, W.S. Contact resistivity and adhesion of copper alloy seed layer for copper-plated silicon heterojunction solar cells. *Jpn. J. Appl. Phys.* **2018**, *57*, 08RB13. [\[CrossRef\]](#)
15. Lee, D.W.; Rehman, A.; Lee, S.H. Characteristics of ITO film dependence upon substrate temperature using electron beam evaporator. *Korean J. Met. Mater.* **2015**, *53*, 729. [\[CrossRef\]](#)
16. Lee, A.R.; Lee, D.W.; Lee, S.H.; Bhopal, M.F.; Kim, H.J.; Lim, K.-J.; Shin, W.-S.; Lee, S.H.; Kim, J. Study of double layer indium tin oxide in silicon hetero-junction solar cells. *J. Nanosci. Nanotechnol.* **2020**, *20*, 161–167. [\[CrossRef\]](#)
17. Chae, M.; Lee, D.; Kim, S.; Kim, H.-D. Improved electrical and optical properties of IGZO transparent conductive oxide due to microwave treatment: Application to silicon solar cells. *IEEE Access* **2022**, *10*, 90401–90407. [\[CrossRef\]](#)
18. Kesmez, Ö.; Akarsu, E.; Çamurlu, H.E.; Yavuz, E.; Akarsu, M.; Arpaç, E. Preparation and characterization of multilayer anti-reflective coatings via sol-gel process. *Ceram. Int.* **2018**, *44*, 3183–3188. [\[CrossRef\]](#)
19. Ye, L.; Ge, X.; Wang, X.; Hui, Z.; Zhang, Y. Design and preparation of durable double-layer non-quarter-wave antireflective coatings. *Ceram. Int.* **2019**, *45*, 8504–8509. [\[CrossRef\]](#)
20. Lee, D.; Kim, H.-D. Improvement in the energy conversion efficiency for silicon heterojunction solar cells due to SiO_x inserted with conducting filaments. *J. Alloys Compd.* **2023**, *932*, 167669. [\[CrossRef\]](#)
21. De, A.; Biswas, P.; Manara, J. Study of annealing time on sol-gel indium tin oxide films on glass. *Mater. Charact.* **2007**, *58*, 629–636. [\[CrossRef\]](#)

22. Zargar, R.A.; Arora, M.; Alshahrani, T.; Shkir, M. Screen printed novel ZnO/MWCNTs nanocomposite thick films. *Ceram. Int.* **2021**, *47*, 6084–6093. [[CrossRef](#)]
23. Lee, D.; Lee, A.; Kim, H.-D. IZO/ITO Double-layered Transparent Conductive Oxide for Silicon Heterojunction Solar Cells. *IEEE Access* **2022**, *10*, 77170–77175. [[CrossRef](#)]
24. Lee, D.W.; Bhopal, M.F.; Lee, S.H.; Lee, A.R.; Kim, H.J.; Rehman, M.A.; Seo, Y.; Lim, K.J.; Shin, W.S.; Lee, S.H. Effect of additional HfO₂ layer deposition on heterojunction c-Si solar cells. *Energy Sci. Eng.* **2018**, *6*, 706–715. [[CrossRef](#)]
25. Yamamoto, K.; Yoshikawa, K.; Uzu, H.; Adachi, D. High-efficiency heterojunction crystalline Si solar cells. *Jpn. J. Appl. Phys.* **2018**, *57*, 08RB20. [[CrossRef](#)]
26. Kim, S.; Balaji, P.; Augusto, A.; Bowden, S.; Honsberg, C.B. Ultra thin Al₂O₃ passivation for hetero-junction Si solar cell. In Proceedings of the 2019 IEEE 46th Photovoltaic Specialists Conference (PVSC), Chicago, IL, USA, 16–21 June 2019; IEEE: Piscataway, NJ, USA, 2019.
27. Ahn, J.; Chou, H.; Banerjee, S.K. Graphene-Al₂O₃-silicon heterojunction solar cells on flexible silicon substrates. *J. Appl. Phys.* **2017**, *121*, 163105. [[CrossRef](#)]
28. Kato, S.; Kurokawa, Y.; Gotoh, K.; Soga, T. Silicon Nanowire Heterojunction Solar Cells with an Al₂O₃ Passivation Film Fabricated by Atomic Layer Deposition. *Nanoscale Res. Lett.* **2019**, *14*, 99. [[CrossRef](#)] [[PubMed](#)]
29. McIntosh, K.R.; Baker-Finch, S.C. OPAL 2: Rapid optical simulation of silicon solar cells. In Proceedings of the 2012 38th IEEE Photovoltaic Specialists Conference, Austin, TX, USA, 3–8 June 2012; IEEE: Piscataway, NJ, USA, 2012; pp. 000265–000271.
30. Double Layer Anti Reflection Coatings. Available online: <https://www.pveducation.org/pvcdrom/design-of-silicon-cells/double-layer-anti-reflection-coatings> (accessed on 26 May 2022).
31. Reference Air Mass 1.5 Spectra. Available online: <https://www.nrel.gov/grid/solar-resource/spectra-am1.5.html> (accessed on 26 May 2022).

Disclaimer/Publisher's Note: The statements, opinions and data contained in all publications are solely those of the individual author(s) and contributor(s) and not of MDPI and/or the editor(s). MDPI and/or the editor(s) disclaim responsibility for any injury to people or property resulting from any ideas, methods, instructions or products referred to in the content.